Potential of Advanced Microwave Sounding Unit-A (AMSU-A) and AMSU-B measurements for atmospheric temperature and humidity profiling over land

Fatima Karbou,[1,2] Filipe Aires,[3] Catherine Prigent,[4] and Laurence Eymard[5]

Received 5 August 2004; revised 1 December 2004; accepted 13 January 2005; published 13 April 2005.

[1] A neural network retrieval method has been applied to investigate AMSU-A/AMSU-B atmospheric temperature and humidity profiling capabilities over land. The retrieval method benefits from a reliable estimate of the land emissivity and skin temperature as well as first guess information regarding the temperature-humidity profiles. It has been applied on a large geographic area (60°W–60°E, 60°S–60°N) and atmospheric situations (winter and summer). The retrieved RMS errors are within 2 K and 9% in temperature and relative humidity, respectively. Regardless of scanning conditions, vegetation types, and atmospheric situations, the algorithm retrieval results are satisfactory for both temperature and relative humidity. The retrieval approach has been evaluated by comparison with available in situ measurements.

Citation: Karbou, F., F. Aires, C. Prigent, and L. Eymard (2005), Potential of Advanced Microwave Sounding Unit-A (AMSU-A) and AMSU-B measurements for atmospheric temperature and humidity profiling over land, *J. Geophys. Res.*, *110*, D07109, doi:10.1029/2004JD005318.

1. Introduction

[2] The Advanced Microwave Sounding Unit-A (AMSU-A) and AMSU-B on board the latest generation of the NOAA polar orbiting satellites measure the outgoing radiances from the atmosphere and the Earth surface. With channels in the oxygen absorption band, AMSU-A is designed to retrieve the atmospheric temperature from about 3 hPa (~45 km) down to the Earth's surface. AMSU-B module makes measurements in the vicinity of the strong water vapor absorption line at 183 GHz and is used for atmospheric water vapor sounding. Therefore the use of AMSU measurements in operational Numerical Weather Prediction (NWP) models can potentially provide accurate monitoring of both air temperature and moisture profiles with good temporal and spatial sampling. Compared to infrared sounding measurements, AMSU observations are less sensitive to high thin and non precipitating clouds.

[3] Several retrieval techniques have been developed for temperature and/or humidity sounding with AMSU-A/AMSU-B and other microwave radiometer measurements. *Rosenkranz* [2001] used surface and atmosphere modeling to retrieve temperature-moisture profiles from AMSU-A/AMSU-B data. *Wagner et al.* [1990] retrieved humidity profiles using passive microwave measurements. A neural network technique has been used by *Shi* [2001] to estimate air temperature profiles from AMSU-A; a similar technique has been utilized by *Franquet* [2003] for 3-D restitution of water vapor using microwave satellite instruments.

[4] Over ocean, the AMSU measurements are now routinely assimilated in NWP systems and they provide unique atmospheric profiling capabilities. Over land however, the AMSU measurements are not fully exploited. At best, only the channels that are not contaminated by surface contributions are assimilated, thus limiting the profiling potential to the higher atmospheric layers. *Kelly and Bauer* [2000] describe the current use of 10 AMSU channels measurement in the European Centre for Medium-Range Weather Forecasts (ECMWF) assimilation system. Recent efforts to assimilate AMSU radiances over ocean/land are performed at many NWP centers (see the proceedings from the Thirteenth International TOVS Study Conference, Sainte-Adèle, Quebec, Canada, 2003, sponsored by International TOVS Working Group and partners). Contrarily to the ocean emissivity, the land surface emissivity is high, often close to unity, leading to difficulties in discriminating between surface and atmosphere contributions. In addition, the land emissivity exhibits complex temporal and spatial variations, depending on surface types, roughness, and moisture content, among other parameters. As a consequence an accurate estimate of the microwave land emissivity is a prerequisite for a full exploitation of satellite sounding measurements over land. Recent works focused on the development and analysis of emissivity estimates at

[1]Centre d'étude des Environnements Terrestre et Planétaires, L'Institut Pierre-Simon Laplace, Centre National de Recherches Scientifiques (CNRS), Vélizy, France.
[2]Now at Centre National de Recherches Météorologiques, Météo-France, CNRS, Toulouse, France.
[3]Laboratoire de Météorologie Dynamique, Institut Pierre-Simon Laplace, CNRS, Palaiseau, France.
[4]Laboratoire d'Étude du Rayonnement et de la Matière en Astrophysique, Observatoire de Paris, CNRS, Paris, France.
[5]Laboratoire d'Océanographie Dynamique et de Climatologie, Institut Pierre-Simon Laplace, CNRS, Paris, France.

0148-0227/05/2004JD005318$09.00

Table 1. AMSU-A and AMSU-B Channel Description

Channel	Frequency, GHz	Noise Equivalent, K	Resolution at Nadir, km
	AMSU-A		
1	23.8	0.20	48
2	31.4	0.27	48
3	50.3	0.22	48
4	52.8	0.15	48
5	53.596 ± 0.115	0.15	48
6	54.4	0.13	48
7	54.9	0.14	48
8	55.5	0.14	48
9	57.290 = f_0	0.20	48
10	f_0 ± 0.217	0.22	48
11	f_0 ± 0.322 ± 0.048	0.24	48
12	f_0 ± 0.322 ± 0.022	0.35	48
13	f_0 ± 0.322 ± 0.010	0.47	48
14	f_0 ± 0.322 ± 0.0045	0.78	48
15	89	0.11	48
	AMSU-B		
16	89	0.37	16
17	150	0.84	16
18	183.31 ± 1	1.06	16
19	183.31 ± 3	0.70	16
20	183.31 ± 7	0.60	16

AMSU frequencies and observation conditions [*Karbou et al.*, 2005], following the method developed for the Special Sensor Microwave/Imager [*Prigent et al.*, 1997, 1998]. It is thus now possible to develop retrieval techniques to fully benefit from microwave sounder measurements over land, as it has already been done for microwave imagers [*Prigent and Rossow*, 1999; *Aires et al.*, 2001].

[5] The objective of this paper is to study the feasibility of use of all AMSU-A and AMSU-B channels over land for retrieving atmospheric temperature and moisture profiles down to the surface; then to evaluate the performances of the retrieval method by quantifying the information content of the AMSU-A and AMSU-B observations for such retrievals over land. The final aim of this study is to investigate and prepare the assimilation (variational method) of all AMSU channel measurements over land in NWP models. The information content analysis is based on neural network (NN) statistical approach, with use of a first guess profile and auxiliary information (surface temperature and emissivity). Compared to more traditional information content techniques [*Rodgers*, 1990], using a NN has the advantage of requiring none of theoretical assumptions such as linearity or the Gaussian character of the variables. Our approach consists in designing a NN retrieval scheme procedure, to apply it to a large set of realistic atmospheric situations, and to analyze the impact of the satellite observations on the retrieved products. Two contrasted months of AMSU data are analyzed over a large part of the globe centered on Africa. In this preliminary study, only cloud free data have been selected to conduct the atmospheric retrievals. Given the scarcity of the radiosonde measurements over large parts of Africa, it is of primary importance to get reliable satellite estimates of the temperature and humidity profiles in this region.

[6] The AMSU observations and the emissivity data set are described in section 2. The retrieval approach is presented in section 3 and its results are analyzed with respect to the AMSU zenith angle, season, and the vegetation type. Additional analysis regarding the ECMWF first guess information is provided in section 4 as well as an evaluation of the retrieval method by comparison with radiosonde measurements. Section 5 concludes this study.

2. Satellite Observations and Emissivity Data Sets

2.1. AMSU-A and AMSU-B Measurements

[7] The AMSU sounding unit operates on board the NOAA satellites since 1998. AMSU-A has 12 channels located close to the oxygen absorption lines below 60 GHz and four window channels at 23.8, 31.4, 50.3, and 89 GHz. AMSU-B has two window channels at 89 and 150 GHz and three channels centered on the 183.31 GHz water vapor line. The two instruments have instantaneous fields of view of 3.3° and 1.1° and sample 30 and 90 Earth views respectively. Therefore the AMSU observation scan angle varies from −48° to +48° with the corresponding local zenith angle reaching 58°. Channel characteristics for both AMSU-A and AMSU-B radiometers are given in Table 1, and a detailed description of the AMSU sounders is reported by *Goodrum et al.* [2000].

[8] Level 1b AMSU data have been obtained from the Satellite Active Archive (SAA) and processed using the Advanced ATOVS Processing Package (AAPP) created and distributed by EUMETSAT and cooperations. The AMSU radiances are corrected from the AMSU antenna effect using coefficients given by *Mo* [1999] and *Hewison and Saunders* [1996]. The analysis in this study is made at AMSU-A spatial resolution. Data have been selected to cover a large geographic area including mainly Africa but also eastern South America, southern Europe, and the Middle East (from 60°W to 60°E in longitude and from 60°S to 60°N in latitude). The study is performed for January and August 2000. At that time, NOAA 15 is in Sun-synchronous polar orbit and crosses the equator at local solar times of approximately 7:30 a.m. and 19:30 p.m.

[9] In the present work, the AMSU information content analysis is conducted over land and under cloud free situations. Once our experience results are thoroughly validated, the analysis will be extended to cloudy situations. Clouds have a complex and highly variable impact on the observed microwave radiances, depending on both the cloud property and the observation frequency. Cloud screening is conducted using the International Satellite Cloud Climatology Project (ISCCP) data sets. Cloud parameters and skin temperatures are extracted from the ISCCP pixel level data (the DX data set) for January and August 2000. These products are available at 30 km ground resolution every 3 hours. Within ISCCP, information about clouds is obtained from visible and infrared measurements from polar and geostationary satellites, using radiative analysis [*Rossow and Schiffer*, 1991].

[10] Figure 1 shows the weighting function distributions for all AMSU channels calculated for a U.S. standard tropical atmosphere at nadir using a microwave radiative transfer model [*Pardo et al.*, 2001]. The weighting functions indicate the relative contribution of each atmospheric layer to the measured radiance. For a given atmosphere and frequency, the peak altitude in the weighting function increases with increasing zenith angle. This is due to increasing optical path length between the satellite and the

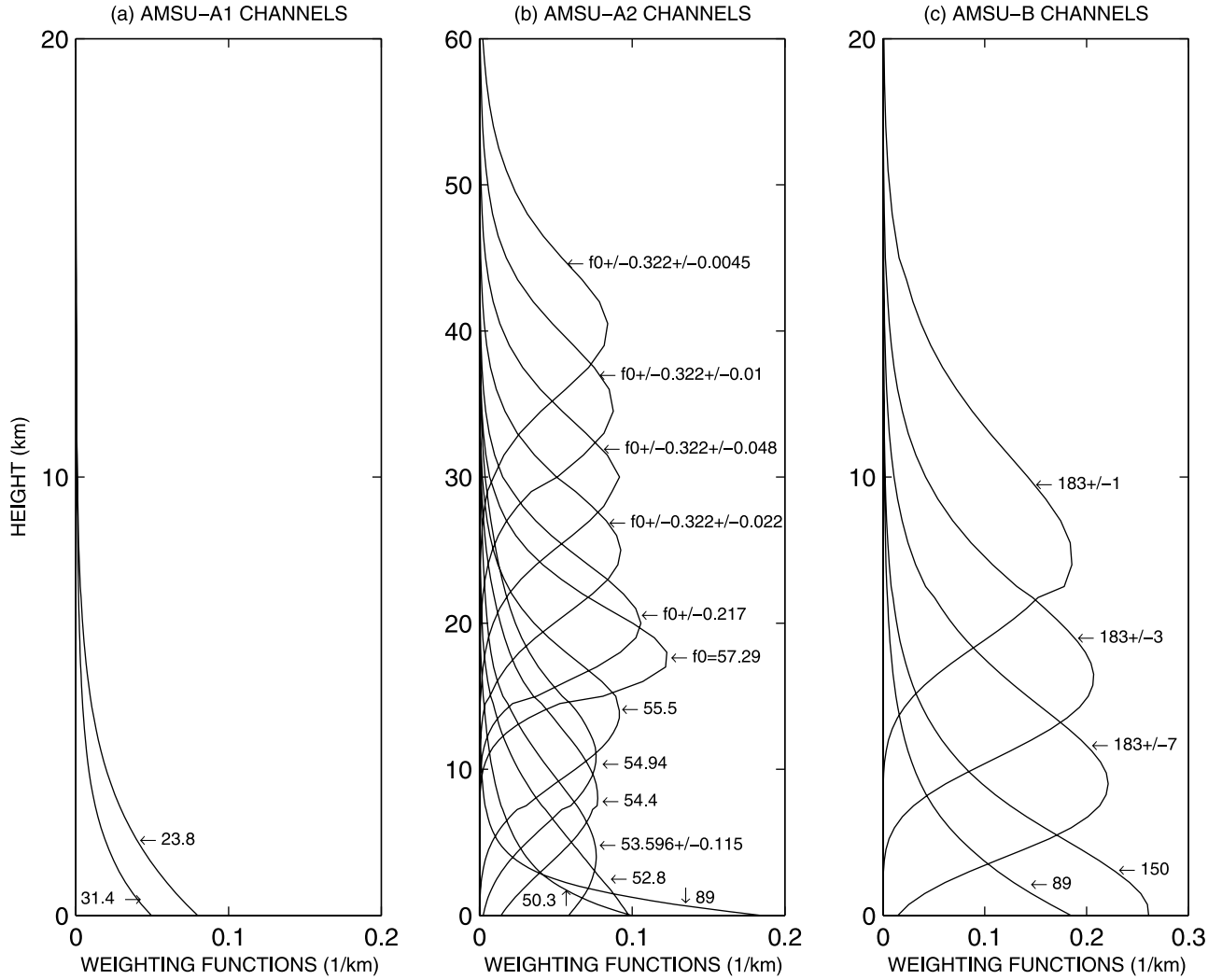

Figure 1. AMSU-A and AMSU-B weighting functions for a U.S. standard tropical atmosphere (WV = 42 kg/m^2) at nadir, assuming a surface temperature of 299 K and a surface emissivity of 0.95 for (a) AMSU-A1, (b) AMSU-A2, and (c) AMSU-B channels.

Earth when the instruments scan from nadir to higher angles. In window channels the weighting function peaks have their maximum closer to the surface. Most of the radiation measured by these window channels comes from the surface and the boundary layer and these channels can be used to derive total precipitable water, precipitation rate, or cloud liquid water over ocean [*Grody et al.*, 2001; *Zhao and Weng*, 2002; *Weng et al.*, 2003]. For all the channels that have some contribution coming from the surface, it is important to accurately estimate the surface emission in order to correctly separate its effect from the atmospheric one.

[11] AMSU observes the Earth with a large range of angles leading to difficulties when developing retrieval algorithms: the angular dependence has to be taken into account in the inversion algorithm. Alternative techniques have been developed to convert the observed radiance at a given angle to the radiance that would be measured at nadir. *Goldberg et al.* [2001], for instance, describe the limb adjustment of AMSU-A observations to nadir. In the present study, no limb correction method is applied. All AMSU-A scan positions are considered and the retrieval accuracy will be evaluated for all angles. Figure 2 shows the mean brightness temperatures (Tbs) against the local zenith angle observed for cloud-free situations in January and August 2000. The observations have been sorted by vegetation types using the biosphere-atmosphere transfer scheme (BATS) vegetation land cover data set (available at 30 × 30 km grid resolution) [*Dickinson et al.*, 1986]. The BATS vegetation classification is a complex combination of three surface climatology classifications obtained from *Matthews* [1983] and *Olson et al.* [1983] and from *Wilson* [1984] as described by *Wilson et al.* [1987a, 1987b]. The angular variations of the Tbs are driven by two phenomena, depending on the channel opacity: for window channels the angular dependence of the emissivity prevails whereas for sounding channels the opacity increase with angle is the dominant effect. Surface and near-surface channel (23.8, 31.4, 50.3, 89.0, and 150 GHz) Tb curves show a similar trend as those observed while analyzing the angular emissivity variation [*Karbou et al.*, 2005]. Figure 3 shows the mean monthly emissivities at 31.4 GHz over desert, calculated for 6 months of data, and sorted out by beam observation

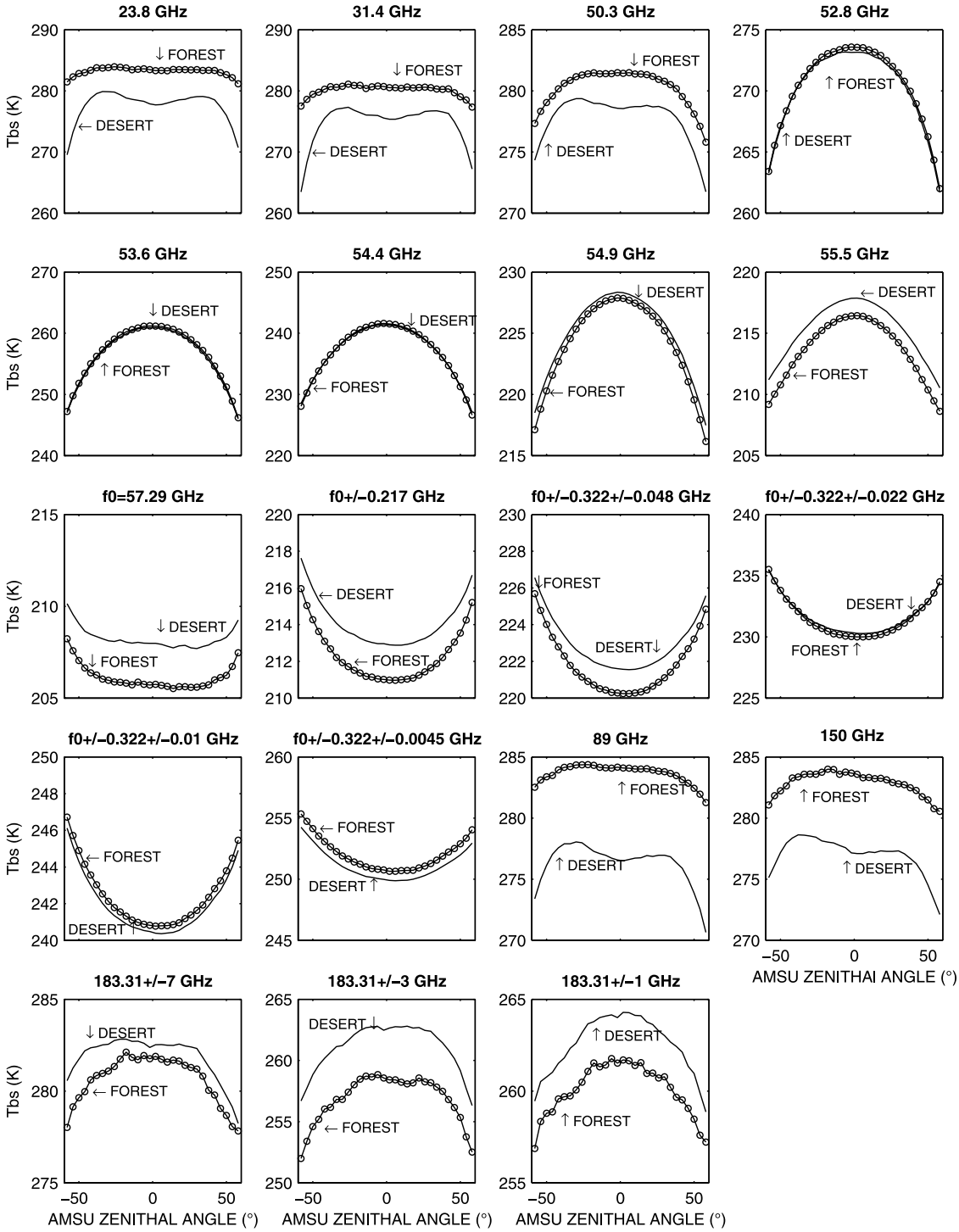

Figure 2. Mean AMSU observed brightness temperatures for January and August 2000 with respect to the zenith angle and two surface types (desert and dense vegetation).

angle; the emissivity curve show similar trend than the mean Tb curve at 31.4 GHz over desert (Figure 2). Most of the angular variations in surface and near-surface channels are related to the surface emissivity angular dependence. *Mo* [2002] made similar observations when comparing mean Tbs and emissivities from AMSU-A channels over the Libyan Desert. As a consequence, an accurate estimate of the emissivity is required for the full incidence angle ranges to properly account for the surface contribution to the measured radiance at each scan angle. For this purpose, the microwave land surface emissivities at AMSU frequencies have been studied [*Karbou et al.*, 2005], and this work is briefly described in section 2.2.

2.2. AMSU Land Emissivity Calculations

[12] The AMSU land surface emissivities have been calculated under the assumption of a flat and specular surface, using data from year 2000, for 30 observation zenith

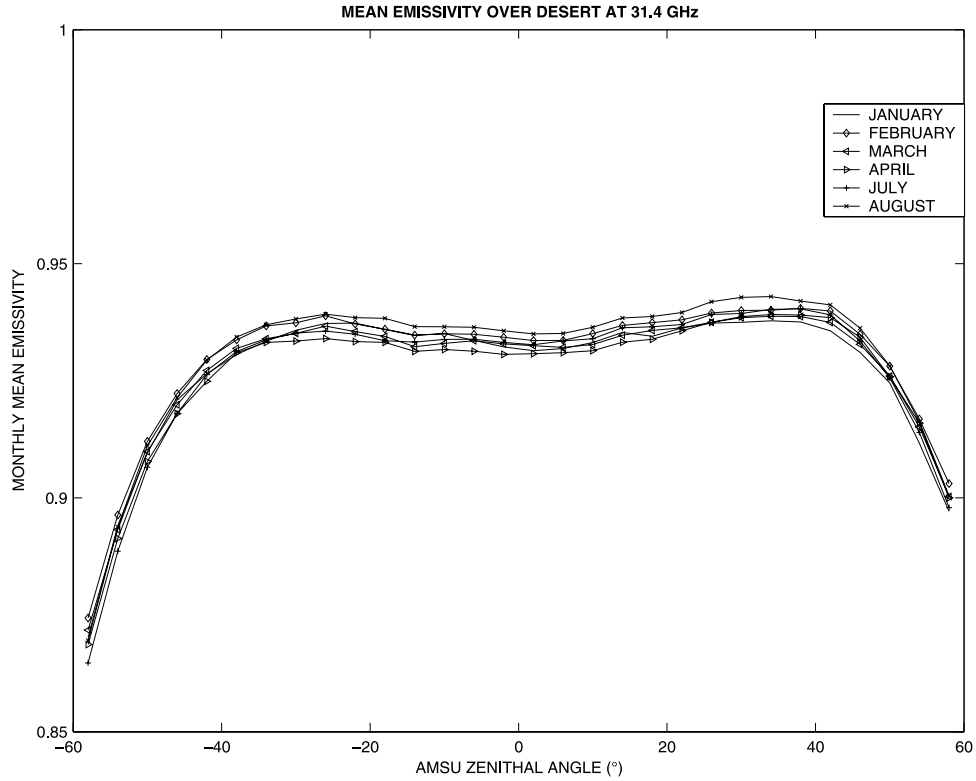

Figure 3. Monthly mean AMSU emissivities at 31.4 GHz for 6 months of data from year 2000 with respect to 30 observation angles and over a desert surface.

angle ranges (from −58° to +58°) and for the 23.8, 31.4, 50.3, 89, and 150 GHz channels after separating cloud and atmospheric contributions [*Karbou et al.*, 2005]. For the emissivity calculations only cloud free data have been considered. Collocated visible/infrared satellite measurements from ISCCP data have been used to screen cloud and rain effects and to provide an accurate estimate of the skin temperature. The nearby temperature-humidity profiles from the ECMWF [*Simmons and Gibson*, 2000] have been used as input into a state-of-the-art microwave radiative transfer model [*Pardo et al.*, 2001] in order to estimate the atmospheric contribution to the measured radiances.

[13] The obtained monthly mean emissivity maps show the expected spatial structures, related to changes in surface types. Lakes and rivers as well as the coastlines are associated with low emissivities at all frequencies but also with high emissivity variability. For the entire data sets, the day-to-day emissivity standard deviations are generally less than 2% in AMSU surface channels and tend to increase with frequency and zenith angles. *English* [1999] showed that the use of land emissivity with accuracy better than 2% would help humidity profile retrievals over land. For all frequencies, the emissivities depend on the incidence angle, especially for bare soil areas. Figure 3 illustrates this angular variation at 31.4 GHz for desert surfaces for 6 months of data. Figure 3 also shows an asymmetry along the AMSU scan, relatively to nadir, variable with frequency and surface emissivity. For all vegetation classes, the AMSU scan asymmetry is found to be higher at 31.4 GHz than at the other frequencies. The maximum scan asymmetry (difference between the monthly mean emissivities at scan position 1 and 30) for this channel reaches up to 3% over desert areas. The 23 GHz channel is also affected by the scan asymmetry but the magnitude of this effect is smaller (2.4 % over desert surfaces). Measurements at 89 GHz appear to be less sensitive to the scan asymmetry than those at 50.3 GHz. *Weng et al.* [2003] also noticed an asymmetry in AMSU surface channels by using AMSU ocean observations and simulations. The AMSU scan asymmetry is likely related to an instrument calibration problem. For effective retrievals of atmospheric variables over ocean and land, the instruments have to be accurately calibrated for all conditions (frequencies and scanning positions). This asymmetry is being investigated in order to suggest adequate corrections. The likely instrumental problem is accounted for by using mean emissivities sorted by scan position. Therefore, in the present study, the observations are systematically sorted out by scan position angle. Precalculated AMSU mean monthly emissivity maps for January and August 2000, with a ground resolution of 30 × 30 km, and at 23, 31, 50, 89 and 150 GHz are used to characterize the land contribution to the measured radiances. The emissivities in the sounding channels have not been calculated because the surface contribution at these frequencies is not strong enough to derive reliable estimates. Given the smooth and limited frequency dependence of the land surface emissivities in this wavelength range [*Prigent et al.*, 2000; *Karbou et al.*, 2005], the emissivities in the window channels can be extrapolated from their estimates in the nearest sounding channels. For example, mean emissivities at 50 GHz have been used for channels in the vicinity of the 50–60 GHz

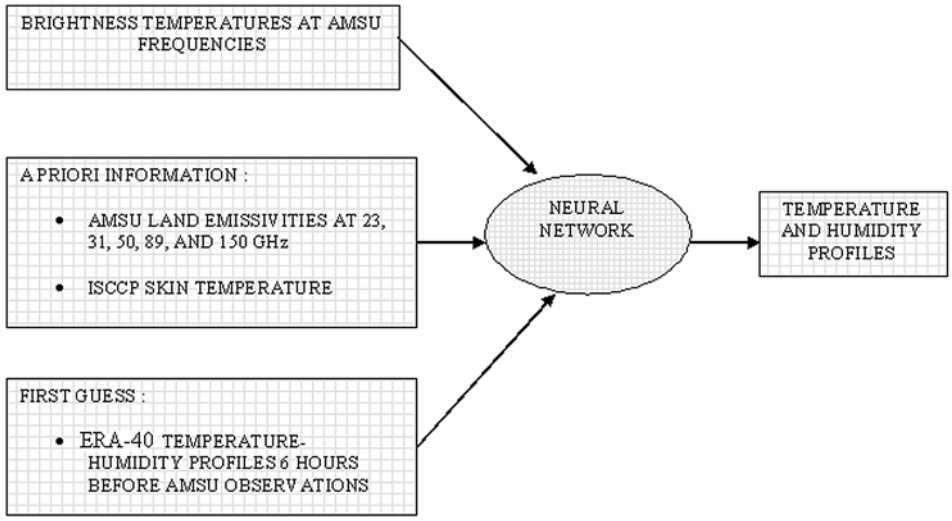

Figure 4. A schematic representation of the neural network scheme.

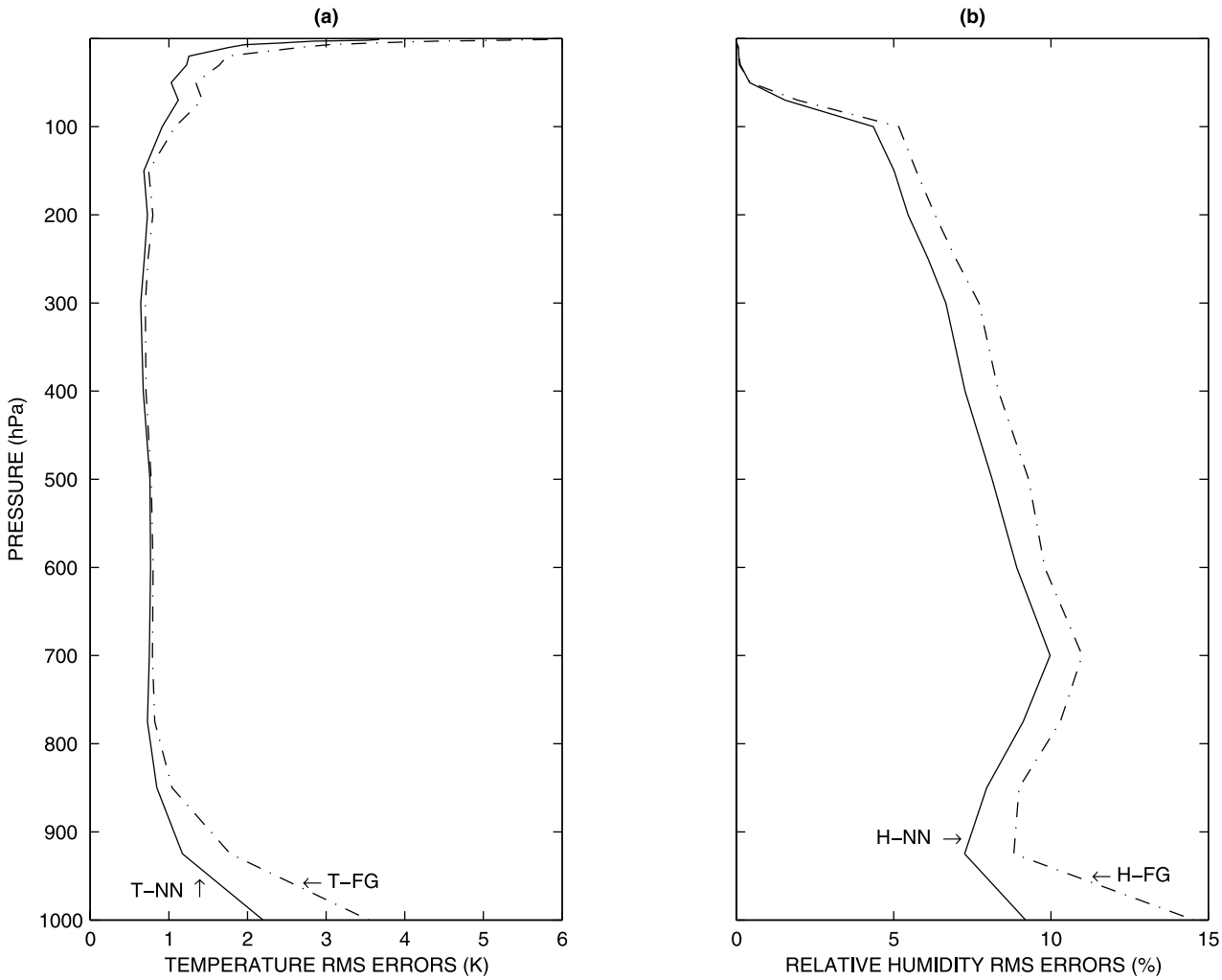

Figure 5. RMS error profiles for the entire database (January and August) for (a) temperature and (b) relative humidity. Dot-dashed lines are for the first guess (FG) error profiles, and solid lines are for the neural network (NN) retrieval error profiles.

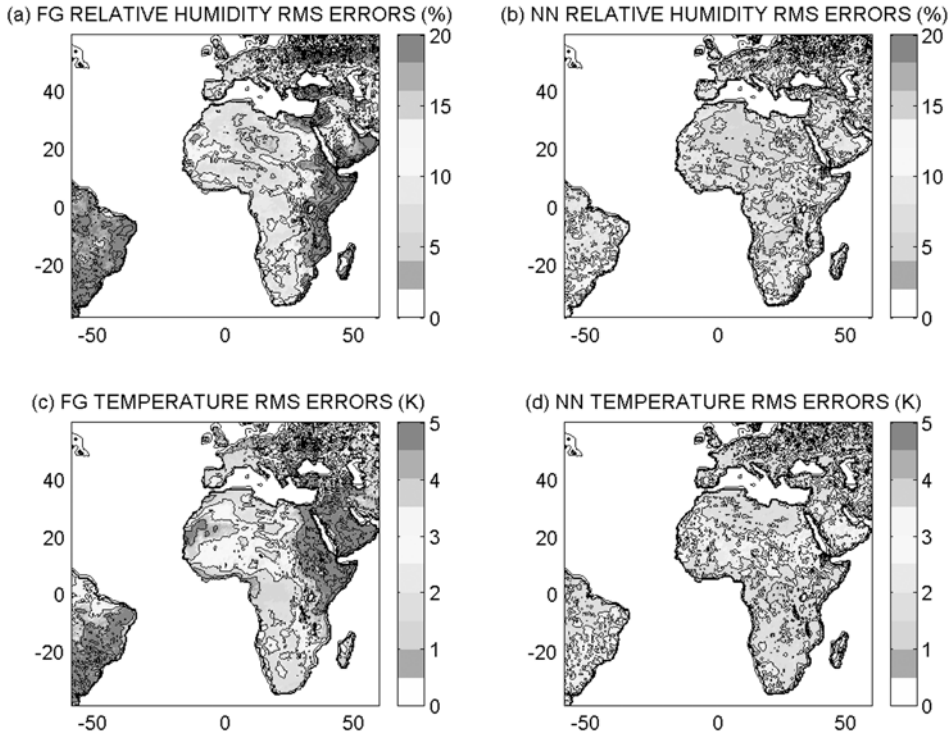

Figure 6. (a) FG RMS error maps at 1000 hPa level for all data and for relative humidity (%). (b) NN RMS error maps at 1000 hPa level for all data and for relative humidity (%). (c) Same as Figure 6a but for temperature (K), and (d) same as Figure 6b but for temperature (K). See color version of this figure in the HTML.

channels band. By the same token, emissivities calculated at 150 GHz have been used for the 183.31 GHz channels.

3. An Information Content Analysis

3.1. Neural Network Approach

[14] The first stage in developing a Neural Network (NN) retrieval scheme is to obtain a data set of samples describing the relationships between the inputs (i.e., satellite observations and a priori information) and the outputs (i.e., variables to retrieve). For this purpose, AMSU measurements and collocated ECMWF reanalyses [*Simmons and Gibson*, 2000] are selected. An alternative would be to simulate AMSU observations with a radiative transfer model using ECMWF atmospheric profiles but in this case the instrument noise would need to be specified, and this information is not directly available in this context. For each AMSU measurement, the closest (in space and time) atmospheric situation from ECMWF to the actual AMSU observation is defined as the target that the NN has to retrieve. Consequently, the procedure includes several sources of observation errors: the instrument noise, differences in space/time collocation, differences in spatial resolution, as well as the error of the ECMWF reanalysis itself related to the NWP model errors.

[15] The NN algorithm is developed to retrieve simultaneously the atmospheric temperature and humidity profiles over land using AMSU-A and AMSU-B observations at 21 fixed pressure levels from 1000 to 1hPa. In addition to satellite measurements, the NN retrieval scheme benefits from other sources of information: a priori and first guess information can be used to better constrain the inversion problem and to limit nonuniqueness and/or instabilities of the solution. This approach was developed by *Aires et al.* [2001] to retrieve simultaneously water vapor, cloud liquid water path, surface temperature, and microwave emissivities over land using SSM/I instrument. In the present study, the three sources of information available to perform the retrieval are: (1) all AMSU-A and AMSU-B satellite observations (i.e., 19 NN inputs corresponding to each instrument frequency), (2) the ECMWF atmospheric temperature and moisture profiles on 21 levels taken 6 hours before the ECMWF target profiles are used as First Guess (FG) information (i.e., 2×21 NN inputs), and (3) spatially and temporally collocated ISCCP skin temperatures as well as the previously calculated emissivities at 23.8, 31.4, 50.3, 89, and 150 GHz are used as a priori information (i.e., 6 NN inputs). The emissivities vary with the geographic location but also with scan position and specified month (January or August). For each channel and each geographic location, the standard deviation of the day-to-day variations within a month has been calculated. The obtained standard deviations are then associated to the mean emissivities during the learning stage. The day-to-day variability of the emissivity is found within 2% for all frequencies [*Karbou et al.*, 2005].

[16] In order to retrieve the temperature and humidity profiles (i.e., 2×21 NN outputs), a multilayered perceptron [*Rumelhart et al.*, 1986] is constructed with 67 inputs, 50 neurons in the hidden layer, and 42 outputs. A schematic structure of the NN inversion scheme is provided in Figure 4.

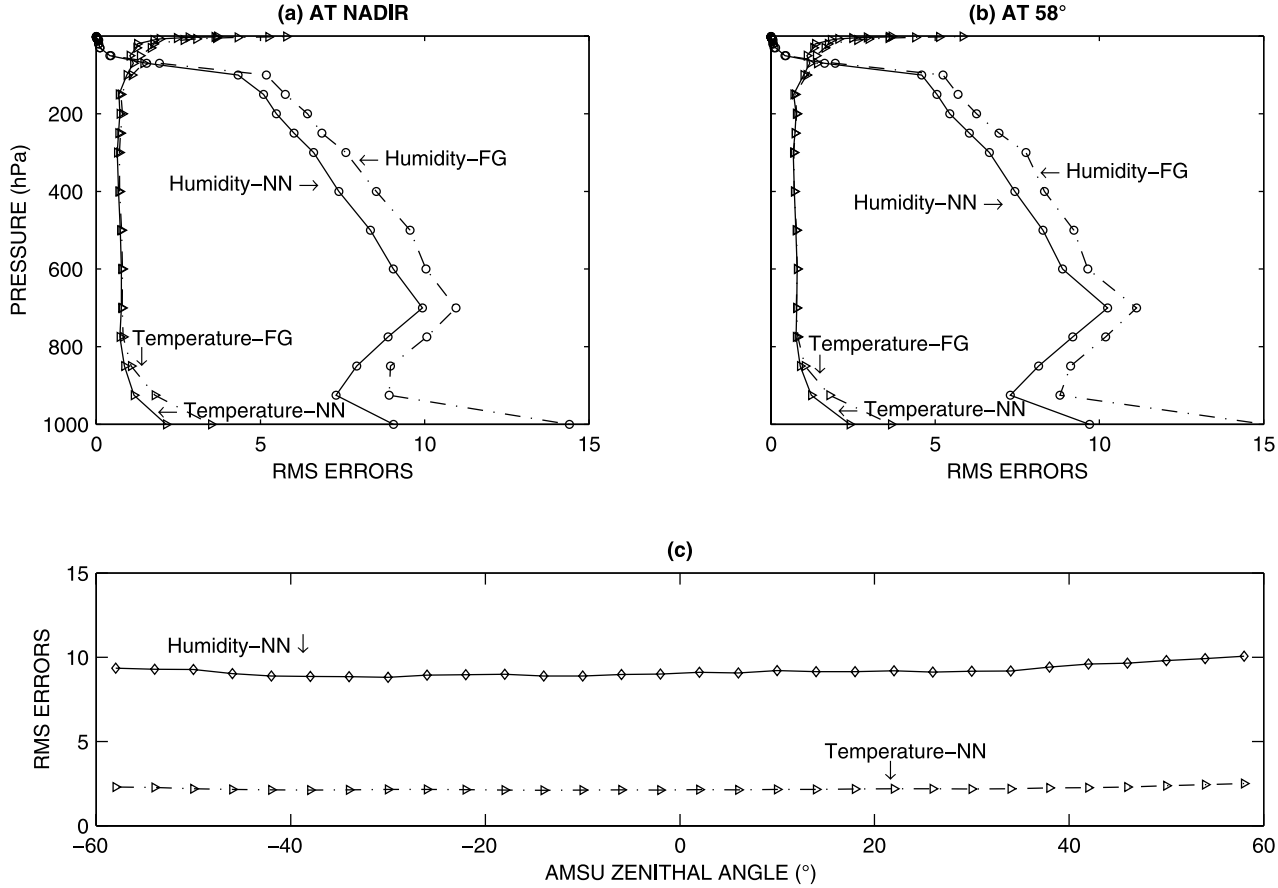

Figure 7. (a) Temperature and humidity RMS error profiles for nadir situations. Both FG and NN error profiles are shown. (b) Same as Figure 7a but at 58° zenith angle. (c) NN RMS errors at 1000 hPa level for both temperature and humidity sorted by AMSU zenith angle.

[17] The data set was constructed using cloud-free AMSU Tbs from January and August 2000 in order to include a wide range of atmospheric conditions. The selected geographic area (60°W–60°E and 60°S–60°N) is large enough to insure variability in surface and atmospheric conditions (from arid to very moist areas). For both August and January months, one third of the data are assigned to the test database whereas two thirds of the data are attributed to the learning database. The applied data repartition allows for a good disjunction between the learning and the generalization data sets. It should be noted that we experimented different database selections (like random daily drawings) and we obtained similar statistics. This confirms the robustness of our estimate of the generalization error.

3.2. Retrieval Results

[18] Figure 5 shows the RMS error profiles for temperature and humidity obtained at 21 pressure levels from 1000 to 1 hPa, regardless of scanning angle, season, and surface types. At each level the FG RMS error profile is calculated using the difference between the target and the FG ECMWF profiles. Similarly, the NN RMS error profile is calculated using the difference between the target and the retrieved profiles. For both temperature and humidity, the retrieved profile is closer to the target profile than the FG profile, showing the benefit of AMSU radiances associated with a reliable characterization of the surface contribution. The improvement in temperature is significant at low (>700 hPa) and at high (<100 hPa) levels: the RMS improvement (difference between the FG and NN RMS errors) is about 1.4 K at 1000 hPa and greater than 0.9 K at levels with pressure lower than 10 hPa. At the lowest level, the RMS errors decrease from 3.5 K to 2.1 K for temperature and from 14.5% to 9.1% in relative humidity. In order to examine the spatial structure of the NN retrieval accuracy, FG and NN RMS error maps are plotted in Figure 6 for both temperature and humidity at 1000 hPa level. Before inversion, the maps of the difference between the FG and the target profile, for both water vapor and temperature, show a very strong longitudinal structure related to the difference between the local time of the satellite overpass and the synoptic times. The FG and target profiles being derived from the reanalysis, they are systematically obtained at the synoptic times (0000, 0600, 1200, or 1800 UTC), and the time difference between these two profiles is always of 6 h. However, this time difference translates into very different temperature or relative humidity differences in the profiles, depending on the local time of the day at the given location. The maps illustrate the NN retrieval improvement with homogenous RMS error over the geographic area to be within 2 K in temperature and 9% in humidity, regardless of the location longitude. In particular, areas with higher FG RMS error in temperature and humidity (i.e., Arabian Desert, South America) are significantly improved by the

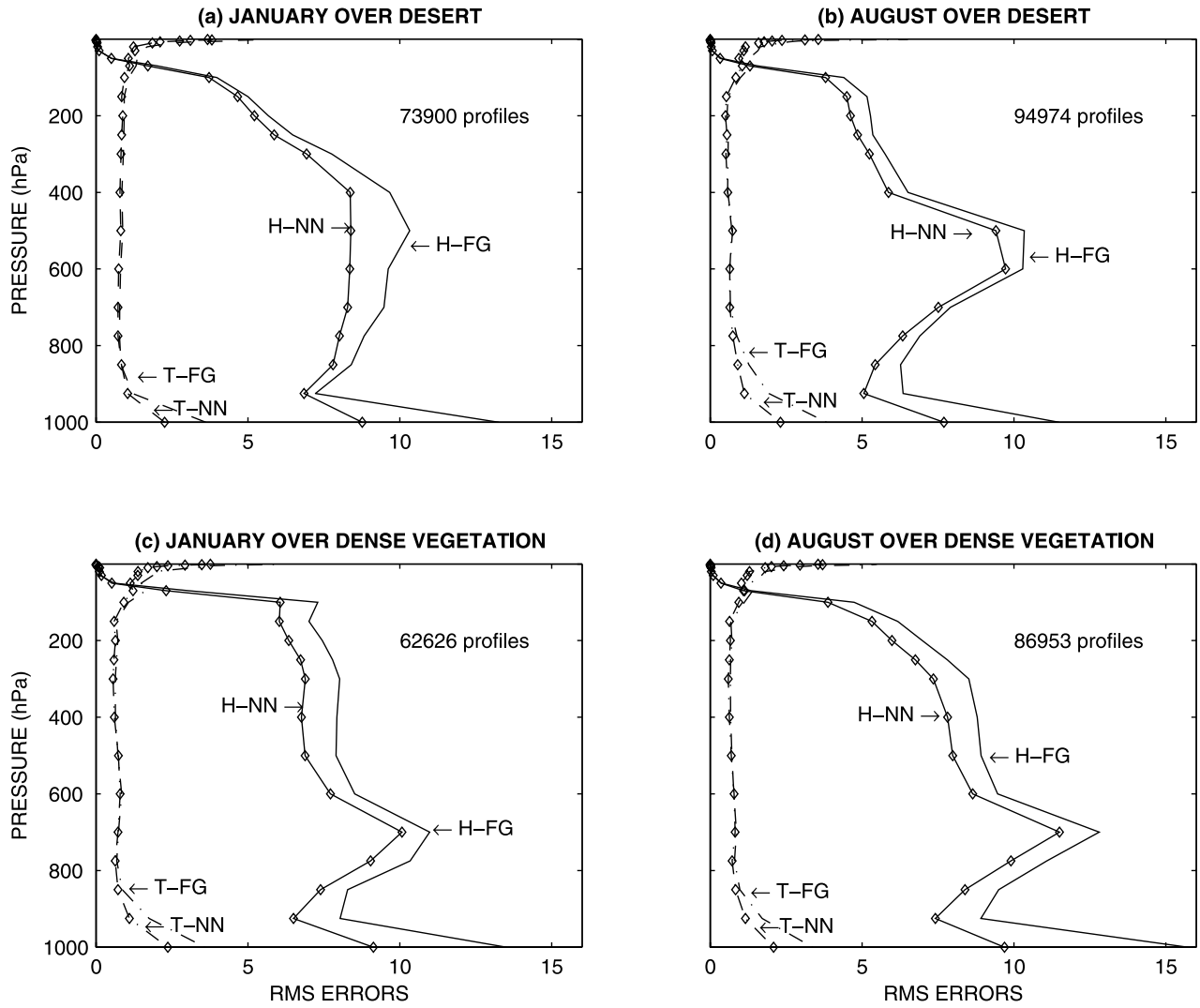

Figure 8. RMS error profiles obtained for both temperature and humidity (FG and NN profiles) for (a) data from January over desert, (b) data from August over desert, (c) data from January over dense vegetation, and (d) data from August over dense vegetation.

NN. There is no significant dependency between the retrieval accuracy and the surface characteristics: The NN retrievals are satisfactory regardless of the surface type.

[19] The previous RMS error profiles have been produced with all data (January and August) and at all AMSU-A scan positions. In the next section, retrieval results are examined more closely with respect to the AMSU-A scan position, the vegetation cover, and the season.

3.3. Scan Angle and Vegetation Dependencies

[20] AMSU-A and AMSU-B instruments scan from −58° to 58° from nadir. The retrieved products are now analyzed to check for scan dependency in the retrieved temperature and humidity profile accuracy. Figure 7 compares the RMS error profiles in temperature and relative humidity at nadir (Figure 7a) and at 58° from nadir (Figure 7b). No significant difference is observed along the profiles between the two scanning cases for both temperature and humidity retrievals. In particular, at surface level, where scan dependencies could likely be the greatest, no significant effect can be noticed. Figure 7c represents the NN RMS errors at 1000 hPa level as a function of the AMSU zenith angle for both temperature and relative humidity, and shows that no significant dependency exists between the surface level RMS errors and the zenith angle for both temperature and humidity. The NN improvement is within 2 K for temperature and 9% for humidity for all scanning situations; in particular, no significant deterioration of the retrievals is observed for high zenith angles. To confirm the retrieval scheme homogenous results with the scan angle, we conducted six retrieval experiments by training six independent NN for six limited ranges of zenith angle ([−58°, −46°], [−42°, −26°], [−22°, nadir], [nadir, 22°], [26°, 42°], and [46°, 58°]). Individual results from these experiments (not shown) do not show better retrieval accuracy than the unique NN.

[21] Retrieved products are now analyzed by season and vegetation characteristics. Figure 8 presents the RMS error profiles for temperature and humidity calculated for desert and dense vegetation areas separately. January and August

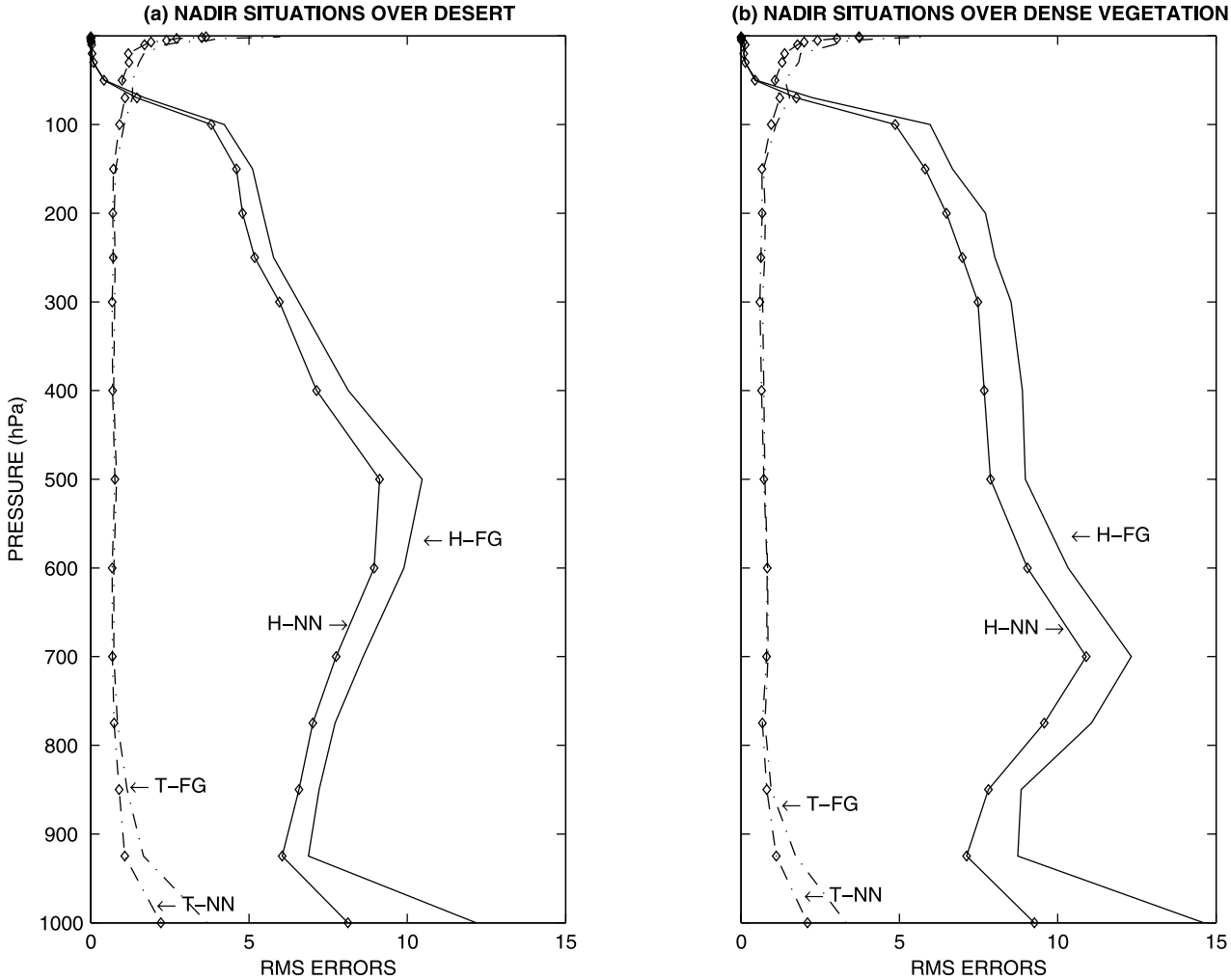

Figure 9. Temperature RMS error (K) and relative humidity RMS error (%) profiles for nadir situations (January and August) obtained for (a) desert and (b) dense vegetation.

data have also been separated and all scanning conditions have been considered. For a given vegetation type, Figure 8 shows homogenous retrieval results for both temperature and humidity, for January and August. A slight improvement of the humidity RMS error at surface level can be noticed in August for desert surfaces. Figure 9 completes this analysis by showing the RMS error profiles of the retrieved parameters over desert and dense vegetation for both January and August, at nadir. The NN retrieval performs well, regardless of season, scanning situations, and vegetation types. The results show that when reliably characterizing the surface, we are able to correctly take into account the surface variability with vegetation and scan observation angle and provides uniformly homogeneous retrievals in very diverse situations, from dry desert regions to very moist equatorial areas. Significant improvements are observed even in the lower atmospheric layers where surface contribution is important.

4. Further Analyses

4.1. On the Role of the Surface

[22] The information content analysis conducted in our study tends to demonstrate the potential of AMSU measurements for atmospheric profiling over land when the surface is well characterized, with both emissivity and skin temperature.

[23] *English* [1999] made a thorough sensitivity analysis of the impact of the emissivity estimate on the humidity and temperature sounding at AMSU frequencies, in the case of variational assimilation. For the humidity sounding he concludes that the emissivity information is very important assuming a good knowledge of the skin temperature. For temperature sounding, the emissivity sensitivity is greater in presence of clouds. The present work relies on this sensitivity analysis and we choose to work in the optimum conditions (regarding the surface description) to perform the information content analysis.

[24] In order to further investigate the role of the emissivity and the skin temperature in the retrieval, a first experiment has been performed to analyze the impact of the emissivity on the brightness temperatures. Tbs have been simulated for one month (August), over a large geographic area, and at all AMSU-A observation angles using (1) reliable emissivity estimations, (2) degraded land emissivities, and (3) using a constant emissivity value (0.95). The results have been analyzed by looking at the differences between Tbs observations and simulations. For

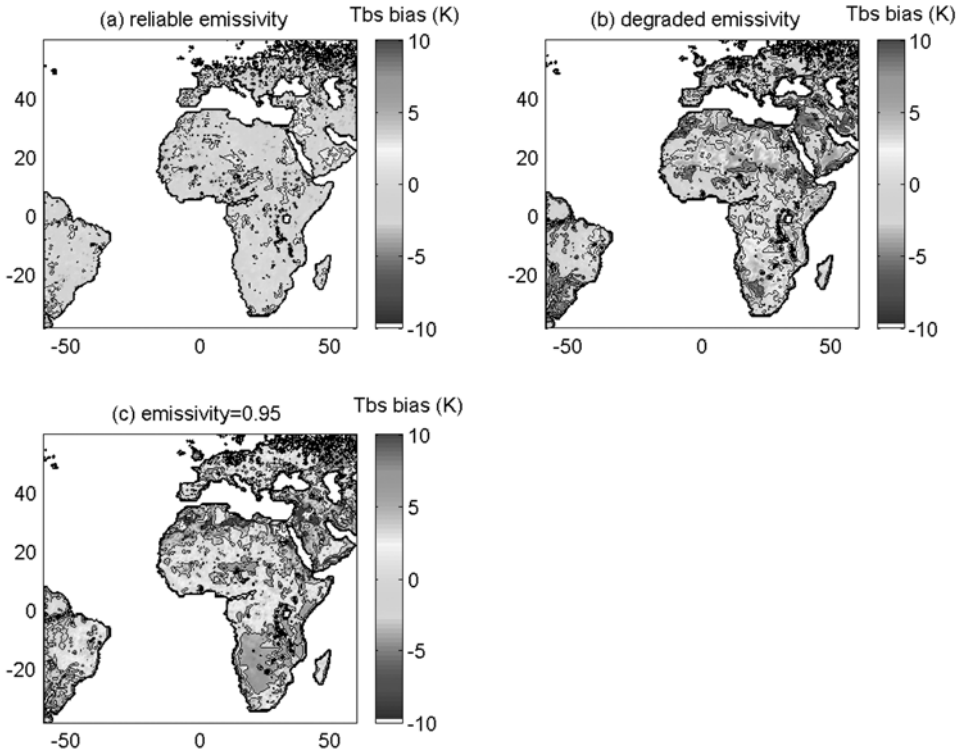

Figure 10. Mean Tbs bias (observations-simulations) maps obtained with August 2000 data, at 23.8 GHz, and using (a) a reliable emissivity estimation, (b) a degraded emissivity data set, and (c) an emissivity equal to 0.95. See color version of this figure in the HTML.

the whole month and the entire geographic area, the global statistics are improved when using a reliable characterization of the emissivity with frequencies and scanning angles. At 31.4 GHz for example, the global statistics (mean/std) are: experiment (1) −0.73/4.45, experiment (2) −0.53/6.43, and experiment (3) −2.67/7.51.

[25] Figure 10 shows the mean Tbs bias (observations-simulations) maps obtained at 23.8 GHz using the three emissivity calculation scenarios described above. The Tbs bias is reduced with the reliable emissivity scenario (Figure 10a), whereas a constant (Figure 10c) or degraded emissivity (Figure 10b) could produce up to ±10 K of bias. These results confirm the impact of the emissivity estimate on the Tbs. Similar calculations could be performed with a degraded skin temperature with similar conclusions.

[26] It is to be noted that in operational mode, the first step consists in a quality control that compares the simulated Tbs (using first guess information) and the measured Tbs. In a recent experiment at ECMWF, in close to operational conditions, a considerable amount of data in channels 5 and 6 passed the control tests using a reliable emissivity estimates and channel 4 could be used as often as channel 5 and 6 whereas it was always rejected using the degraded emissivity estimates [*Prigent et al.*, 2005]. Using reliable emissivity estimate significantly increases the number of satellite observations that are assimilated in the system, making it possible then to use them.

[27] Further sensitivity analysis to both skin temperature and emissivity estimates have to be performed in order to investigate their impact on temperature-humidity retrievals in both clear and cloudy situations, in the context of Neural Network inversion. This is the objective of our further work.

4.2. Impact of the First Guess Temperature and Humidity Profiles

[28] The previous analysis shows that by using temperature and relative humidity first guess profiles (i.e., ECMWF profiles 6 hour before the target ECMWF profile, called FG-06) along with accurate surface skin temperature and emissivities, the surface effect on the AMSU measurements can be decorrelated from the atmospheric one leading to atmospheric temperature/humidity retrievals over land. In this section we examine the impact of the FG profiles choice on the NN retrievals. This is achieved by training NNs using the same AMSU data set but with two different FG scenarios: First, using ECMWF profiles 24 hours before AMSU observations (called FG-24) and second, using the closest profile to the AMSU observation time but with additive noise (called FG-NOISE). The noise characteristics are those of the ECMWF model in 2000; these characteristics have been revised since. For specific humidity, the specification of the standard deviations is established using several statistics including radiosonde observations and it depends on the atmospheric situations [*Rabier et al.*, 1998]. On the contrary, temperature standard deviations only vary with latitude (i.e., different specifications for each 10° latitude range). The relative humidity noise is calculated for each ECMWF profile taking into account the temperature, specific humidity, and pressure. The temperature noise is calculated for

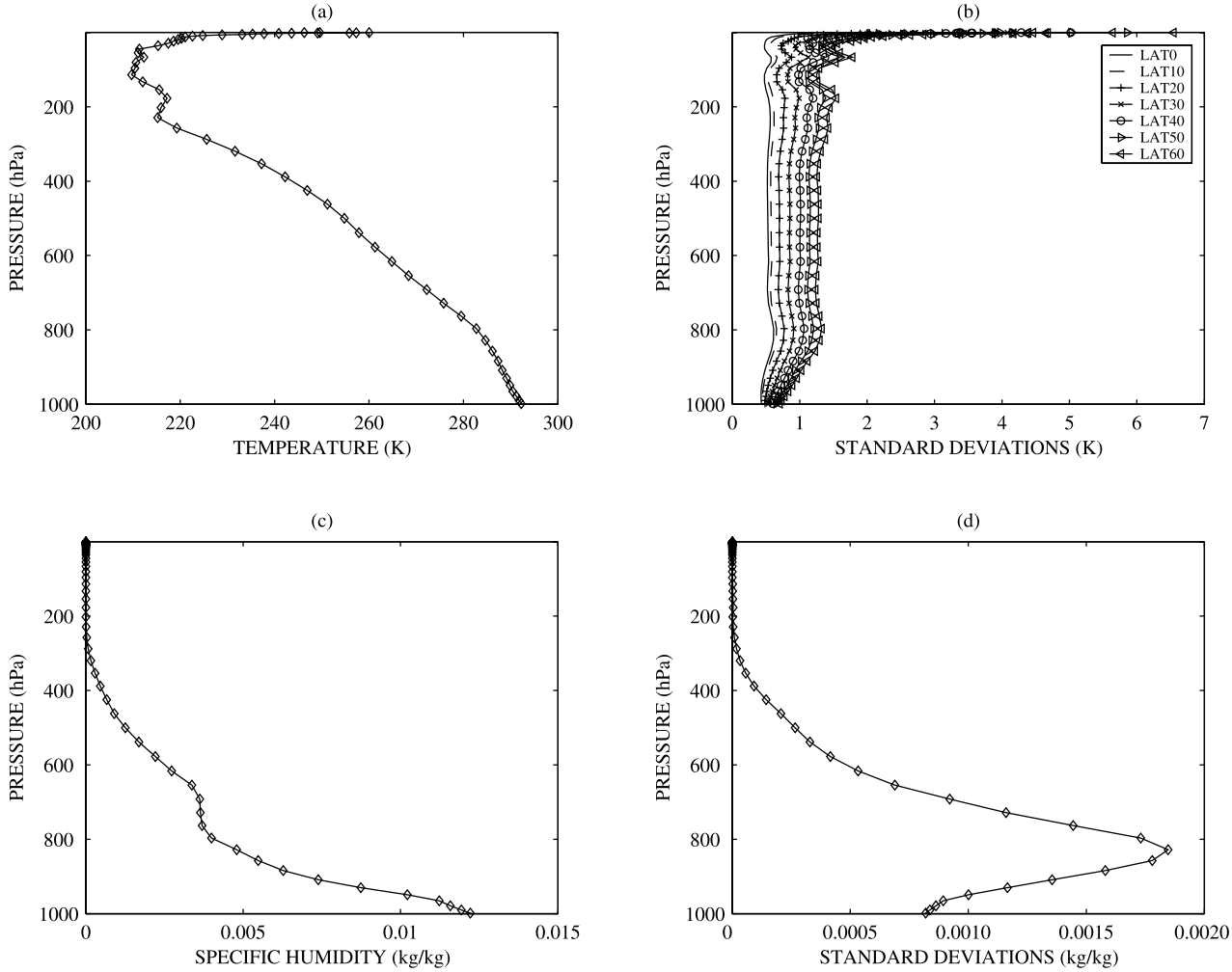

Figure 11. Sample temperature-humidity profile from the study database (a and c) and the corresponding standard deviations for (b) temperature assuming different latitude ranges and (d) specific humidity.

ranges of latitudes over the studied area corresponding to (0°–10°, 10°–20°, 30°–40°, 40°–50°, and 50°–60°). Figure 11 shows a temperature-humidity profile from our database (Figures 11a and 11c) and the corresponding standard deviations for temperature assuming different latitudes (Figure 11b) and specific humidity using *Rabier et al.*'s [1998] method (Figure 11d).

[29] Figures 12a–12c present the temperature and relative humidity NN results for the different FG scenarios: the RMS error profiles are plotted for the three FG configurations and for the corresponding NN retrievals. For temperature, the FG-24H is of less quality than the FG-06H, except for lower levels where the diurnal variability can be higher than the day-to-day changes. The FG-NOISE is always better than FG-06H and FG-24H with standard deviation of errors already close to 0.5 K for each vertical layer: Not surprisingly, in the FG-NOISE configuration, the use of AMSU satellite observations in the retrieval scheme slightly improves the FG especially at high pressure levels; it can even degrade it in the lower levels. For our retrieval method, The FG-06H and FG-24H configurations appear more adequate and the retrieval at FG-06H has better statistics than the FG-24H. For relative humidity, all FG scenarios seem to be adequate for our retrieval algorithm, and in all cases the FG is improved by the NN retrieval. Best humidity retrievals are obtained using the FG-06H and FG-NOISE scenarios. From this set of experiments, it can be seen that retrieval results are highly dependent on the FG profiles choice. In our information content analysis, the temperature/humidity FG-06 scenario seems to be a good compromise: the obtained statistics are satisfactory for both temperature and humidity retrievals (especially at atmospheric low levels).

4.3. Retrieval Method Evaluation With Radiosonde Data

[30] Radiosonde observations provide independent and unique reference for temperature and humidity profiles that can be used for satellite retrieval validation. However, their use for such evaluation has some recognized limitations. For instance, they are unevenly distributed over the Earth with different measurement accuracy. They are particularly scarce in Africa. Measurements are performed at fixed times generally twice a day. They represent 1D information up to

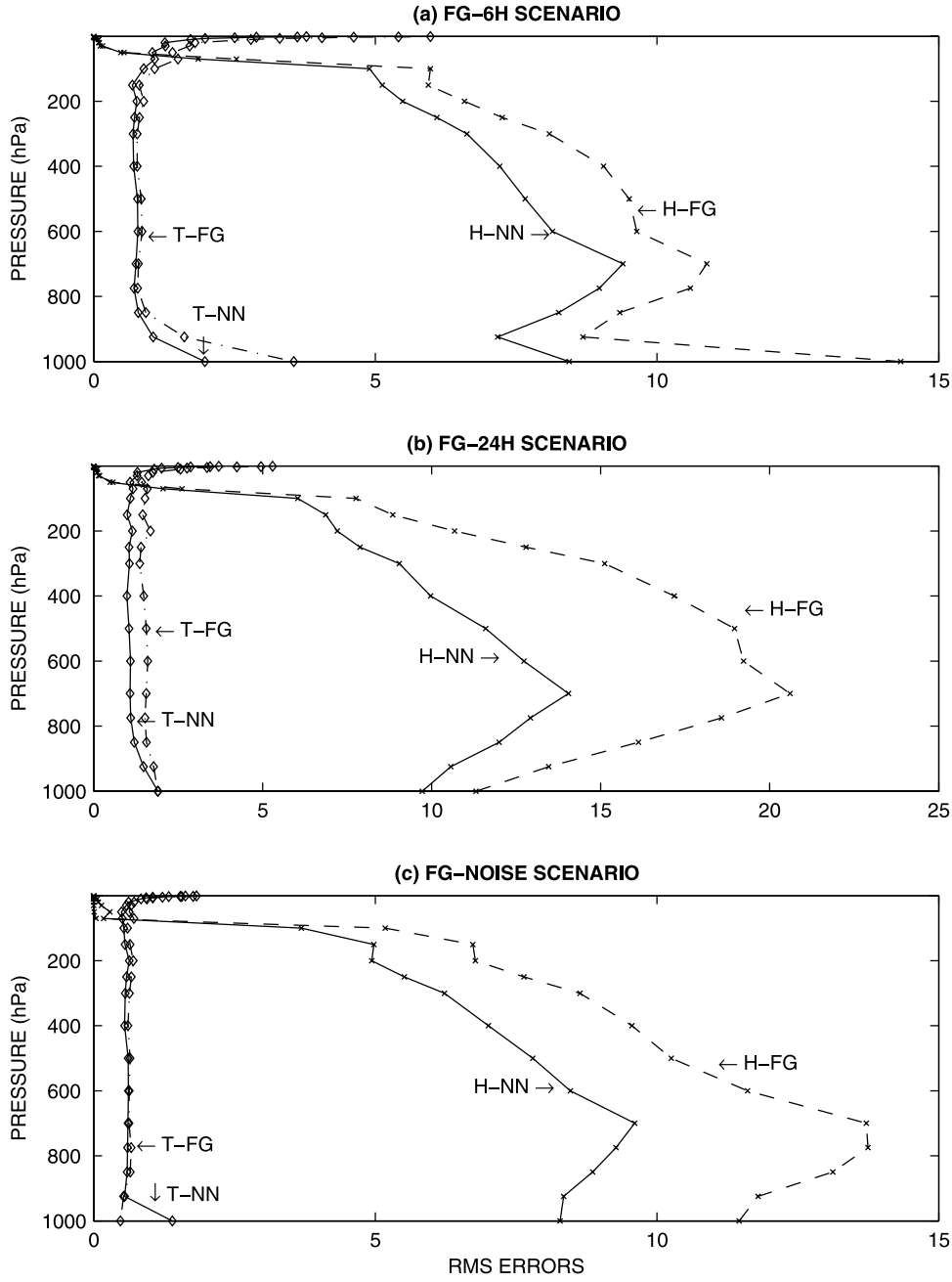

Figure 12. The RMS error profiles obtained for the entire database using different ECMWF FG profile scenarios for temperature and relative humidity.

generally 100hPa whereas the satellite measures a large atmospheric volume, from the bottom to the top of the atmosphere and with the horizontal spatial extent related to the instrument field of view.

[31] Records of radiosonde measurements are archived at many meteorological centers. For example, global radiosonde data sets from 1998 to 2004 are produced jointly by the National Climatic Data Center (NCDC, http://www.ncdc.noaa.gov) and the Forecast Systems Laboratory (FSL, http://www.fsl.noaa.gov). Radiosonde stations located within the studied geographic area (60°W–60°E and 60°S–60°N) and operational during January and August 2000 have been collocated in space and time with AMSU observations. Table 2 lists the selected radiosonde stations with their locations. These stations produce daily temperature and humidity profiles at 0000 and at 1200 UTC. During 2000, only the NOAA 15 satellite was operational with equator crossing at 7:30 a.m. and 19:30 p.m. As a consequence, there is at least 3 hours difference between the AMSU and selected radiosonde observation times.

[32] Figure 13 shows the RMS error profiles obtained by comparing the FG and the NN retrieval with the collocated radiosonde measurement. As expected, the FG errors as compared to radiosondes are rather large, but we already commented in the beginning of this section on the limitations of radiosonde comparisons, in particular considering the

Table 2. Selected FSL/NCDC Radiosonde Stations

WMO Station	Location	Country	Latitude, deg	Longitude, deg	Height, m
075100	Bordeaux/Merignac	France	44.83	−0.70	45
076450	Nimes/Courbessac	France	43.86	04.40	60
080010	La Coruna	Spain	43.36	−08.41	67
080230	Santander	Spain	43.46	−03.81	79
084300	Murcia	Spain	37.98	−01.11	54
084950	North Front	Gibraltar	36.15	−05.35	3
161440	S. Pietro Capofiume	Italy	44.65	11.61	38
162450	Pratica di Mare	Italy	41.65	12.43	12
166220	Thessaloniki/Mikra	Greece	40.51	22.96	7
167160	Athens/Hellenikon	Greece	37.90	23.73	14
170300	Samsun	Tunisia	41.28	36.33	44
170620	Istanbul/Goztepe	Tunisia	40.96	29.08	40
172200	Izmir	Tunisia	38.43	27.16	25
173510	Adana/Bolge	Tunisia	37.05	35.35	27
401000	Beirut/Khalde International	Lebanon	33.81	35.48	16
401790	Bet Dagan	Israel	32.00	34.81	30
410240	Jeddah/Abdul-Aziz	Saudi Arabia	21.66	39.15	20
603900	Alger/Dar El Beida	Algeria	36.71	03.25	23
607150	Tunis Carthage	Tunisia	36.83	10.23	5
620100	Tripoli International	Libya	32.90	13.28	80
620530	Benina	Libya	32.08	20.26	39
623060	Mersa Matruh	Egypt	31.33	27.21	28
623370	El Arish	Egypt	31.08	33.75	32
623780	Helwan	Egypt	29.86	31.33	139
649100	Douala observatory	Cameroon	04.01	09.70	10
655780	Abidjan/Port Bouet	Ivory Coast	05.25	−03.93	6
685880	Durban/Louis Botha	South Africa	−29.96	30.95	8

large space and time differences in the collocation process. Since the FG RMS error profiles include large collocation errors, the detection of a relative improvement is difficult. At surface level however, the RMS error is improved by about 2 K in temperature and 2.5% in humidity. This confirms that, when associated to careful design of retrieval technique, AMSU-A and AMSU-B observations can help retrieve low-level temperature and humidity profiles over land.

5. Summary and Conclusions

[33] This paper studied the feasibility of AMSU temperature and humidity profile retrieval over land, down to the surface. A neural network retrieval algorithm was developed, in which the AMSU satellite observations were combined with a priori surface skin temperature and surface emissivity, and with first guess information on the atmospheric profiles. The retrieval method has been applied over a large geographic area including mainly Africa but also eastern South America, southern Europe, and the Middle East (from 60°W to 60°E in longitudes and from 60°S to 60°N in latitudes). A very large number of atmospheric situations have been considered for our experiment, from a winter and a summer month. The NN retrievals over this large data set is used as an information content analysis aiming at the evaluation of the potential of AMSU observations in improving low-level temperature and humidity profiles over land.

[34] Results are encouraging: the RMS errors at surface level are within 2 K in temperature and 9% in relative humidity. A sensitivity study has been conducted to analyze the sensitivity of the retrieval algorithm with season, vegetation type, and scan angle: The NN method, when correctly trained on a large data set and using the adequate surface emissivity and skin temperature description, is able to account for the large variability of the situations and to provide accurate atmospheric temperature and humidity profiles over land. We attempted to assess the quality of our retrieval approach by comparison with available radiosonde data. At surface level, the RMS errors are improved (by comparison with radiosonde profiles) by about 2 K in temperature and 2.5% in humidity in all cases. These results confirm that, when combined with reliable estimates of the land emissivity and the skin temperature, AMSU observations are a valuable source of information for the characterization of low-level temperature and humidity profiles over land. The natural continuation of this work will therefore involve the variational assimilation of such products in a NWP model.

[35] Over Africa, the obtained AMSU derived profiles are of great interest because of the insufficient number of radiosonde stations in this continent. In a future work, additional radiosonde validation will be performed during a period when more NOAA satellites are operational: this should help improve the temporal collocation with the radiosonde measurements. The African Monsoon Multidisciplinary Analyses (AMMA) program could be a great opportunity for further radiosonde validation. This program is an international effort to help understand the West African Monsoon and its implication from local to global scales regarding the physical, chemical, and biological environments. The so-called ''extended operation period'' of AMMA in 2005–2007 will be based on the densification of radiosonde and other local measurements over West Africa. A better collocation of radiosonde and AMSU observations will help assess the impact of AMSU measurements on temperature and humidity retrievals.

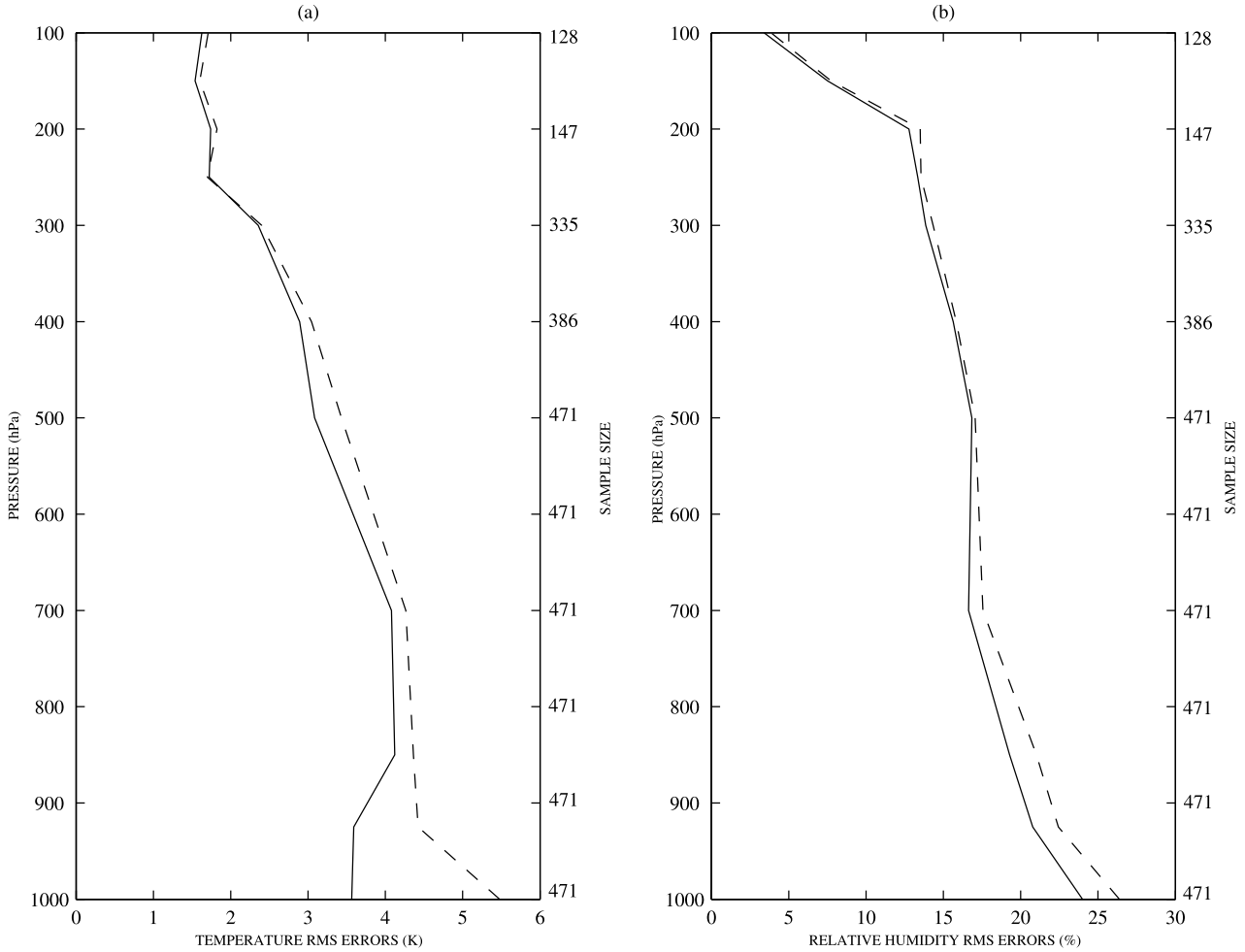

Figure 13. (a) RMS error profiles obtained by comparison to radiosonde measurements for temperature. The dashed line is for the FG, and the solid line is for the NN retrieval. (b) Same as Figure 13a but for relative humidity. The number of radiosonde measurements is also indicated on the right axis.

[36] Once thoroughly validated, the extension of the algorithm to the globe will be investigated. A similar algorithm designed for cloudy scenes will also be developed, benefiting from the experience already acquired with the SSM/I instrument [*Aires et al.*, 2001].

[37] **Acknowledgments.** The authors wish to thank Frederic Chevalier for his help at different stages of this work and for valuable discussions regarding AMSU instruments, ECMWF products and noise characteristics. They also appreciate discussions with Fuzhong Weng regarding AMSU calibration. The authors are very grateful to Christian Mätzler and an anonymous reviewer for detailed and helpful comments about the manuscript. They would like to thank Sophie Cloche and Jean Louis Monge for their help to archive and process the ERA40 and AMSU data. The ISCCP data have been provided by Bill Rossow, AMSU data via the SAA and ERA40 from ECMWF.

References

Aires, F., C. Prigent, W. B. Rossow, and M. Rothstein (2001), A new neural network approach including first guess for retrieval of atmospheric water vapor, cloud liquid water path, surface temperature, and emissivities over land from satellite microwave observations, *J. Geophys. Res.*, *106*, 14,887–14,907.

Dickinson, R. E., A. Henderson-Sellers, P. J. Kennedy, and M. F. Wilson (1986), Biosphere-atmosphere transfer scheme (BATS) for the NCAR community climate model, *Tech. Note NCAR/TN275+STR*, 69 pp., Natl. Cent. for Atmos. Res., Boulder, Colo.

English, S. (1999), Estimation of temperature and humidity profile information from microwave radiances over different surface types, *J. Appl. Meteorol.*, *38*, 1526–1541.

Franquet, S. (2003), Contribution à l'étude du cycle hydrologique par radiométrie hyperfréquence: Algorithmes de restitution (réseaux de neurones) et validation pour la vapeur d'eau (instruments AMSU, SAPHIR) et les précipitations (AMSU, Radarsau sol Baltrad), doctoral thesis, Univ. Paris-Diderot (Paris VII), Paris, 3 March.

Goldberg, M. D., D. S. Crosby, and L. Zhou (2001), The limb adjustment of AMSU-A observations: Methodology and validation, *J. Appl. Meteorol.*, *40*, 70–83.

Goodrum, G., K. B. Kidwell, and W. Winston (2000), NOAA KLM user's guide, NOAA, Silver Spring, Md.

Grody, N. C., J. Zhao, R. Ferraro, F. Weng, and R. Boers (2001), Determination of precipitable water and cloud liquid water over oceans from the NOAA-15 advanced microwave sounding unit, *J. Geophys. Res.*, *106*, 2943–2954.

Hewison, T., and R. W. Saunders (1996), Measurements of the AMSU-B Antenna Pattern, *IEEE Trans. Geosci. Remote Sens.*, *34*, 2, 405–412.

Karbou, F., C. Prigent, L. Eymard, and J. Pardo (2005), Microwave land emissivity calculations using AMSU-A and AMSU-B measurements, *IEEE Trans. Geosci. Remote Sens.*, in press.

Kelly, G., and P. Bauer (2000), The use of AMSU-A surface channels to obtain surface emissivity over land, snow and ice for numerical weather prediction, paper presented at the Eleventh International TOVS Study Conference, Int. TOVS Work. Group, Budapest, Hungary.

Matthews, E. (1983), Global vegetation and land use: New high resolution data bases for climate studies, *J. Clim. Appl. Meteorol.*, *22*, 474–486.

Mo, T. (1999), AMSU-A antenna pattern corrections, *IEEE Trans. Geosci. Remote Sens.*, *37*, 103–112.

Mo, T. (2002), A study of the NOAA 16 AMSU-A brightness temperatures observed over Libyan Desert, *J. Geophys. Res.*, *107*(D14), 4226, doi:10.1029/2001JD001158.

Olson, J. S., J. A. Watts, and L. J. Allison (1983), Carbon in live vegetation of major world ecosystems, *Rep. DOE/NBB–0037 TR004*, 152 pp., U.S. Dep. of Energy, Washington, D. C.

Pardo, J. R., J. Cernicharo, and E. Serabyn (2001), Atmospheric transmission at microwave (ATM): An improved model for millimetre/submillimeter applications, *IEEE Trans. Antennas Propag.*, *49*, 1683–1694.

Prigent, C., and W. B. Rossow (1999), Retrieval of surface and atmospheric parameters over land from SSM/I: Potential and limitation, *Q. J. R. Meteorol. Soc.*, *125*, 2379–2400.

Prigent, C., W. B. Rossow, and E. Matthews (1997), Microwave land surface emissivities estimated from SSM/I observations, *J. Geophys. Res.*, *102*, 21,867–21,890.

Prigent, C., W. B. Rossow, and E. Matthews (1998), Global maps of microwave land surface emissivities: Potential for land surface characterization, *Radio Sci.*, *33*, 745–751.

Prigent, C., J.-P. Wigneron, W. B. Rossow, and J. R. Pardo-Carrion (2000), Frequency and angular variations of land surface microwave emissivities: Can we estimate SSM/T and AMSU emissivities from SSM/I emissivities?, *IEEE Trans. Geosci. Remote Sens.*, *38*, 2373–2386.

Prigent, C., F. Chevallier, F. Karbou, P. Bauer, and G. Kelly (2005), AMSU-A surface emissivities for the ECMWF assimilation, *J. Appl. Meteorol.*, in press.

Rabier, F., A. McNally, E. Andersson, P. Courtier, P. Undén, J. Eyre, A. Hollingsworth, and F. Bouttier (1998), The ECMWF implementation of three-dimensional variational assimilation (3D-Var). II Structure functions, *Q. J. R. Meteorol. Soc.*, *124*, 1809–1829.

Rodgers, C. D. (1990), Characterization and error analysis of profiles retrieved from remote sounding measurements, *J. Geophys. Res.*, *95*, 5587–5595.

Rosenkranz, P. (2001), Retrieval of temperature and moisture profiles from AMSU-A and AMSU-B measurements, *IEEE Trans. Geosci. Remote Sens.*, *39*, 2429–2435.

Rossow, W. B., and R. A. Schiffer (1991), ISCCP cloud data products, *Bull. Am. Meteorol. Soc.*, *72*, 2–20.

Rumelhart, D. E., G. E. Hinton, and R. J. Williams (1986), Learning internal representations by error propagation, in *Parallel Distributed Processing: Explorations in the Microstructure of Cognition*, vol. I, *Foundations*, edited by D. E. Rumelhart, J. L. McClelland, and the PDP Research Group, pp. 318–362, MIT Press, Cambridge, Mass.

Shi, L. (2001), Retrieval of atmospheric temperature profiles from AMSU-A measurements using a neural network approach, *J. Atmos. Oceanic Technol.*, *18*, 340–347.

Simmons, A. J., and J. K. Gibson (2000), The ERA-40 project plan, *ERA-40 Proj. Rep. Ser. 1*, 62 pp., Eur. Cent. for Medium-Range Weather Forecasts, Reading, U. K.

Wagner, D., E. Ruprecht, and C. Simmer (1990), A combination of microwave observations from satellites and an EOF analysis to retrieve vertical humidity profiles over the ocean, *J. Appl. Meteorol.*, *29*, 1142–1157.

Weng, F., L. Zhao, R. Ferraro, G. Poe, X. Li, and N. Grody (2003), Advanced Microwave Sounding Unit cloud and precipitation algorithms, *Radio Sci.*, *38*(4), 8068, doi:10.1029/2002RS002679.

Wilson, M. F. (1984), The construction and use of land surface information in a general circulation climate model, Ph.D. thesis, 346 pp., Univ. of Liverpool, Liverpool, U. K.

Wilson, M. F., A. Henderson-Sellers, R. E. Dickinson, and P. J. Kennedy (1987a), Investigation of the sensitivity of the land-surface parameterization of the NCAR community climate model in region of tundra vegetation, *J. Climatol.*, *7*, 319–343.

Wilson, M. F., A. Henderson-Sellers, R. E. Dickinson, and P. J. Kennedy (1987b), Sensitivity of the biosphere-atmosphere transfer scheme (BATS) to the inclusion of variable soil characteristics, *J. Clim Appl. Meteorol.*, *26*, 341–362.

Zhao, L., and F. Weng (2002), Retrieval of ice cloud parameters using the Advanced Microwave Sounding Unit (AMSU), *J. Appl. Meteorol.*, *41*, 384–395.

F. Aires, Laboratoire de Météorologie Dynamique, IPSL, CNRS, F-91128 Palaiseau Cedex, France.

L. Eymard, Laboratoire d'Océanographie Dynamique et de Climatologie, IPSL, CNRS, Boîte 100, 4, place Jussieu, F-75252 Paris Cedex 05, France.

F. Karbou, Centre National de Recherche Météorologiques, Météo-France, CNRS, 42 avenue de Coriolis, F-31057 Toulouse Cedex, France. (fatima.karbou@cnrm.meteo.fr)

C. Prigent, Laboratoire d'Étude du Rayonnement et de la Matière en Astrophysique, Observatoire de Paris, CNRS, 61 avenue de l'Observatoire, F-75014 Paris, France.